Polymer Chemistry

ROYAL SOCIETY OF CHEMISTRY

PAPER

View Article Online
View Journal | View Issue

Cite this: *Polym. Chem.*, 2025, **16**, 4537

Control over Ba(II)-mediated single-chain polymer nanoparticle compaction by dynamic metal complexation

Sebastian Gillhuber, †[a,b,c] Jochen A. Kammerer, †[b,c] Ada Quinn, †[d,e] Joshua O. Holloway, [b,c] Kai Mundsinger, [b,c] Evelina Liarou, [f] Dmitri Golberg, [b,c] Hendrik Frisch, [b,c] Megan L. O'Mara, *[d,e] Christopher Barner-Kowollik *[b,c,g,h] and Peter W. Roesky *[a,g]

Received 9th September 2025,
Accepted 11th September 2025

DOI: 10.1039/d5py00883b

rsc.li/polymers

The current study investigates the dynamic interactions of barium ions with a synthetic polymer, leading to the formation of intramolecularly folded single-chain nanoparticles (SCNPs), providing targeted control over the polymer morphology. Understanding of the experimental findings is aided by sophisticated molecular dynamics simulations. The high contrast provided by the heavy metal ions within the barium-functionalized nanoparticles enables the scanning transmission electron microscopy (STEM) imaging of single metal atoms within individual SCNPs. The reported findings are expected to aid the in-depth understanding of metal polymer interactions in general. The newly developed concepts hold key potential for the investigation of structure–property relationships of metallopolymers in an unprecedented fashion.

Introduction

In his famous 1959 speech "There's plenty of room at the bottom", Richard Feynman outlined his vision of "manipulating and controlling things on the small scale".[1] Before and after, the field of nanotechnology has fascinated scientists and over the years has evolved to a versatile playground for various fields of research. One area of particular interest is the synthesis and application of nanoparticles. In general, nanoparticles are substances with a spatial extent of less than 100 nm in at least one dimension.[2] Taking inspiration from naturally occurring proteins, which form nanosized particles with unique, outstanding properties from a linear strand of amino acids *via* intramolecular interactions, the field of single-chain nanoparticles (SCNPs) has emerged. SCNPs are constructed from individual synthetic macromolecular chains by intramolecular interactions of complementary functional groups, resulting in more compact morphologies compared to the precursor macromolecules.[3] Intramolecular single-chain folding is commonly based on covalent[4–18] or non-covalent[19–25] interactions,[3] and the folding units can either be randomly distributed along the polymer chain, commonly referred to as repeat unit folding, or be located at predefined positions, referred to as selective point folding.[26]

Following the design principles of natural metalloproteins, our groups and others have focused on the metal functionalization of SCNPs, allowing to synergistically combine the tuneable characteristics of polymeric materials with the diverse functionalities of metal complexes inspired by nature's perfection.[27–52] The precise location and distribution of metal ions within individual SCNPs can exert a critical influence on their function.[27] However, contemporary analytical methods provide little to no insights on the distribution of the metal functionalities within individual macromolecules.

Achieving on-demand control over polymer morphology is one of the driving forces of polymer chemistry in general and the SCNP field in particular. Especially intriguing is the targeted manipulation of the folding and unfolding process of individual macromolecular chains. Consequently, apart from

[a]*Institute of Inorganic Chemistry, Karlsruhe Institute of Technology (KIT), Engesserstraße 15, 76131 Karlsruhe, Germany. E-mail: roesky@kit.edu*
[b]*School of Chemistry and Physics, Queensland University of Technology (QUT), 2 George Street, 4000 Brisbane, QLD, Australia. E-mail: christopher.barnerkowollik@qut.edu.au*
[c]*Centre for Materials Science, Queensland University of Technology (QUT), 2 George Street, 4000 Brisbane, QLD, Australia*
[d]*Australian Institute of Bioengineering and Nanotechnology, The University of Queensland, St Lucia, QLD, Australia. E-mail: m.omara@uq.edu.au*
[e]*ARC Industry Transformation Training Centre for Cryo-electron Microscopy of Membrane Proteins (CCeMMP), Australia*
[f]*Department of Chemistry, University of Warwick, Coventry CV4 7AL, UK*
[g]*Institute of Nanotechnology (INT), Karlsruhe Institute of Technology (KIT), Hermann-von-Helmholtz-Platz 1, 76344 Eggenstein-Leopoldshafen, Germany*
[h]*Institute of Functional Interfaces (IFG), Karlsruhe Institute of Technology (KIT), Hermann-von-Helmholtz-Platz 1, 76344 Eggenstein-Leopoldshafen, Germany. E-mail: christopher.barner-kowollik@kit.edu*
† These authors contributed equally.

SCNP folding, the reverse process of SCNP unfolding triggered by external stimuli has gained significant attention in recent years.[53] Various external triggers have been investigated, including mechanical force,[54,55] temperature[56] or pH changes,[15,57] disruption of self-assembly or host–guest interactions by chemical triggers[58–60] or electrochemically,[61] redox reactions,[62] or even light[63–65] and further studied in computational work.[66,67] Within the above listed examples, only two systems are based on the on-demand reversion of metal polymer interactions.[54,57]

In the current study, we introduce the synthesis of SCNPs folded *via* dynamic interactions with Ba(II) ions (refer to Fig. 1). The dynamic nature of the interactions is demonstrated by sophisticated molecular dynamics simulations and experimentally verified by exploiting the well-established chemistry of barium in aqueous solution, thereby achieving targeted control over the SCNP folding state. The high scanning transmission electron microscopy (STEM) contrast provided by the heavy metal ions present within our Ba(II) SCNPs enables the imaging of metal atoms within individual SCNPs with single-atom sensitivity.

Results and discussion

Single-chain polymer compaction by Ba(II) complexation

Initially, a statistical copolymer of poly(ethylene glycol) methyl ether methacrylate (PEGMEMA, average M_n = 300 g mol^{-1}) and 2-carboxyethyl acrylate (Polymer **P1**) was synthesized by reversible addition–fragmentation chain transfer polymerization (RAFT). While PEGMEMA provides solubility in polar solvents, such as water, the carboxylic acid groups of the 2-carboxyethyl acrylate moieties enable the simple and efficient post-polymerization modification of **P1**. Given the statistical nature of the described copolymerization process, all SCNP folding reactions reported herein follow the repeat unit approach.[26] A number-average molar mass of M_n = 48 700 g mol^{-1} and dispersity of $Đ$ = 1.5 were determined for **P1** by size-exclusion chromatography (SEC) measurements in tetrahydrofuran (THF). Analysis of the ^{1}H nuclear magnetic resonance (NMR) spectrum of **P1** indicates a content of close to 14% 2-carboxyethyl functionalities per macromolecular chain (refer to SI Chapter 3). Ba(II)-mediated single-chain polymer compaction to form **SCNP1-Ba** was achieved by slow addition of a solution of **P1** in water to an aqueous solution of barium hydroxide octahydrate (refer to Fig. 1). The basic nature of the barium hydroxide octahydrate ensured the quantitative deprotonation of the carboxylic acid functionalities in **P1**. However, considering the high dilution of the polymer solution, the carboxylic acid groups were expected to be deprotonated even in the absence of a strong base according to Ostwald's dilution law.

On a functional group level, the conversion of the carboxylic acid functionalities of **P1** to carboxylate groups within **SCNP1-Ba** was confirmed by infrared (IR) spectroscopy (refer to Fig. 2a). It is noted in passing that quantitative comparison of IR data is to be considered with caution, however, the qualitative differences between the spectra are unambiguous. A decrease in the intensity of the carbonyl band at $\tilde{\nu}_{C=O}$ = 1724 cm^{-1}, accompanied by the emergence of two new bands for the asymmetric carboxylate vibration at $\tilde{\nu}_{as,COO}$ = 1583 cm^{-1} and the symmetric carboxylate vibration at $\tilde{\nu}_{s,COO}$ = 1410 cm^{-1}, respectively, is evident.[68] The carbonyl band did not vanish completely as carbonyl groups are also part of the ester bonds in the side chains of **P1**, which remain virtually uninfluenced by the SCNP folding process to **SCNP1-Ba**.

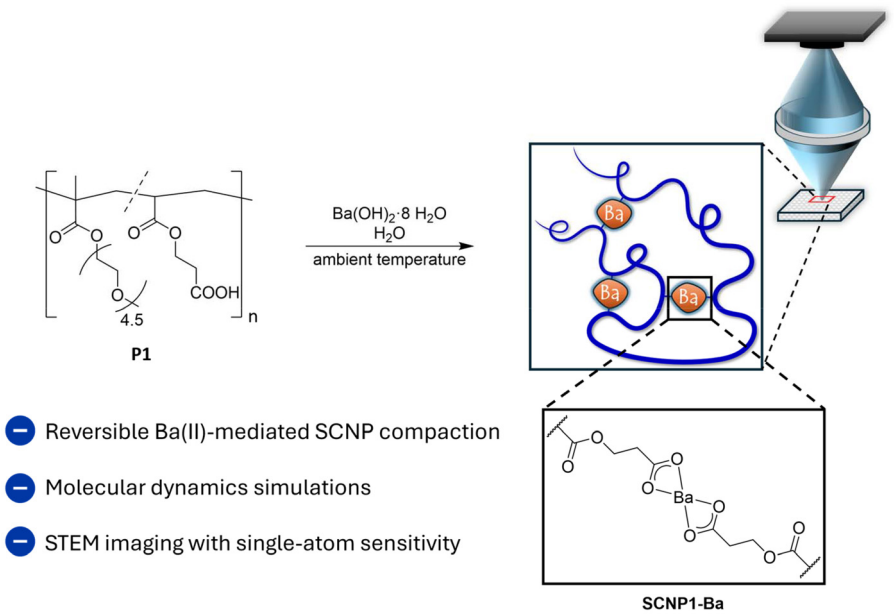

Fig. 1 Schematic illustration of the synthesis of **SCNP1-Ba** from polymer **P1**.

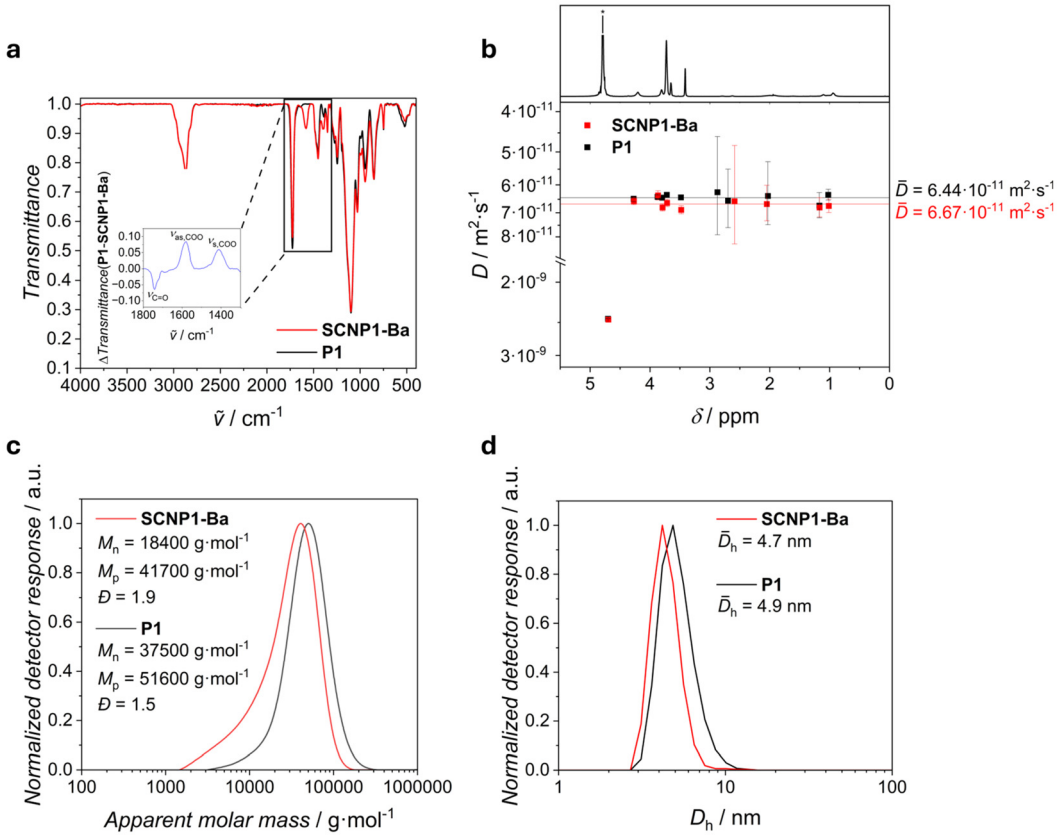

Fig. 2 Analytical confirmation of the Ba(II)-mediated folding of polymer **P1** (black) to **SCNP1-Ba** (red). (a) Superimposed FT-IR (ATR) spectra. Insert shows the difference in transmittance (blue) between **P1** and **SCNP1-Ba** obtained by subtraction of the respective transmittance spectra in the selected region. (b) Superimposed ^{1}H DOSY NMR spectra (400 MHz, D_2O, 313 K). Spectral trace on top refers to **P1**. Error bars refer to data fitting error. Horizontal lines indicate average diffusion coefficients. Asterisk denotes residual solvent resonance. (c) Superimposed SEC chromatograms (THF, RI, PMMA cal.). (d) Superimposed number-weighted DLS size distributions (H_2O, mean diameter by number, average values derived from five measurements).

SCNP formation is based on the introduction of intramolecular crosslinks to individual macromolecular chains. However, IR spectroscopy is incapable of differentiating between intramolecular crosslinking, required for SCNP formation, and undesirable intermolecular interactions. Thus, size-sensitive techniques were employed to verify the successful intramolecular collapse of **P1** upon reaction with Ba(II) ions to form **SCNP1-Ba**. Successful SCNP compaction was evident from diffusion-ordered ^{1}H NMR spectroscopy (DOSY) in D_2O (refer to Fig. 2b), revealing an increase of the average diffusion coefficient of **SCNP1-Ba** (D = 6.67 × 10^{-11} m^2 s^{-1}) with respect to **P1** (D = 6.44 × 10^{-11} m^2 s^{-1}), in line with the expected decrease in the hydrodynamic volume of the polymer particles upon single-chain folding. The molar mass distribution of **SCNP1-Ba** obtained by SEC in THF is shifted towards lower apparent molar masses compared to the corresponding distribution of **P1**, again evidencing single-chain compaction (refer to Fig. 2c and SI Fig. S5). The derived number-average and peak molar masses decreased from M_n = 37 500 g mol^{-1} and M_p = 51 600 g mol^{-1} for **P1** to M_n = 18 400 g mol^{-1} and M_p = 41 700 g mol^{-1} for **SCNP1-Ba**. Concomitantly, the dispersity changed from $Đ$ = 1.5 (**P1**) to $Đ$ = 1.9 (**SCNP1-Ba**). This trend was corroborated by dynamic light scattering (DLS) measurements in water (refer to Fig. 2d), showing a decrease of the number-average hydrodynamic diameter from D_h = 4.9 nm for **P1** to D_h = 4.7 nm for **SCNP1-Ba**.

To explore the effect of the barium loading on the compaction process, the SCNP folding reaction was conducted in the presence of different amounts of barium hydroxide octahydrate at a constant polymer concentration. As a trend, the compaction is less pronounced at lower barium loadings (refer to SI Fig. S2).

To ensure that the observed compaction is indeed based on the coordination of polymer-bound carboxylate functionalities to barium ions and is not caused by alterations of intramolecular hydrogen bonding interactions due to the presence of barium ions, a styrene-based model system with significantly reduced abilities for intramolecular hydrogen bonding compared to **P1** was synthesized. Detailed characterization of this model system (**P2**/**SCNP2-Ba**) in THF revealed that Ba(II)-induced SCNP folding also occurs in systems in which alterations in intramolecular hydrogen bonding due to the presence

of barium ions are not expected to play any significant role (refer to SI Chapter 5).

Molecular dynamics simulations reveal dynamic metal polymer interactions

To deepen the understanding of the interactions of the Ba(II) ions with polymer **P1**, united atom molecular dynamics simulations were performed. Briefly, different starting conformations were generated[69] and their interactions with Ba(II) ions in water[70] investigated. Computational details are provided within the SI (Chapter 6).

The simulations revealed a dynamic nature of the metal polymer interactions, with the barium ions constantly binding to and unbinding form the macromolecules across the simulation trajectories. On average, a given Ba(II) ion was in contact with at least one functional group of the macromolecule for about 66% of the simulation time (refer to SI Table S8). SI Table S6 shows the distribution of the number of barium ions bound to a macromolecular chain over the simulation frames, indicating that the majority of SCNPs featured six to fourteen barium ions per nanoparticle under the employed conditions. The barium ions were found to be surrounded by two defined coordination spheres (refer to SI Fig. S22). Coordination of functional groups of the polymer to the innermost coordination sphere was rare and short lived, accounting for less than 1.5% of the total simulation time (refer to SI Table S8). Instead, the majority of metal polymer interactions took place in the second coordination sphere, whereas the first coordination sphere was dominantly populated by solvent molecules. While interactions of ether and ester oxygen atoms of the polymer side chains with the Ba(II) ions occurred (refer to SI Tables S11–S13), metal binding was predominantly achieved *via* the carboxylate groups (refer to SI Table S9). Carboxylate oxygen atoms were found within the second coordination sphere of the barium ions in more than 80% of all metal polymer interactions (refer to Fig. 3a and SI Table S9). In over 25% of cases, more than one carboxylate group was coordinated to a given barium ion (refer to Fig. 3b–d and SI Tables S9 and S10). Notably, these bridging interactions occurred more frequently in systems with an extended starting conformation (12% of all metal polymer interactions) than in systems with a compact starting conformation (8% of all metal polymer interactions), whereas the frequency of all metal polymer interactions proved to be independent of the initial chain conformation. In extremely rare cases, accounting for about 0.2% of all metal polymer interactions, ten or more PEG side chain ether oxygen atoms were present in the second coordination sphere of the barium ions (refer to SI Table S11).

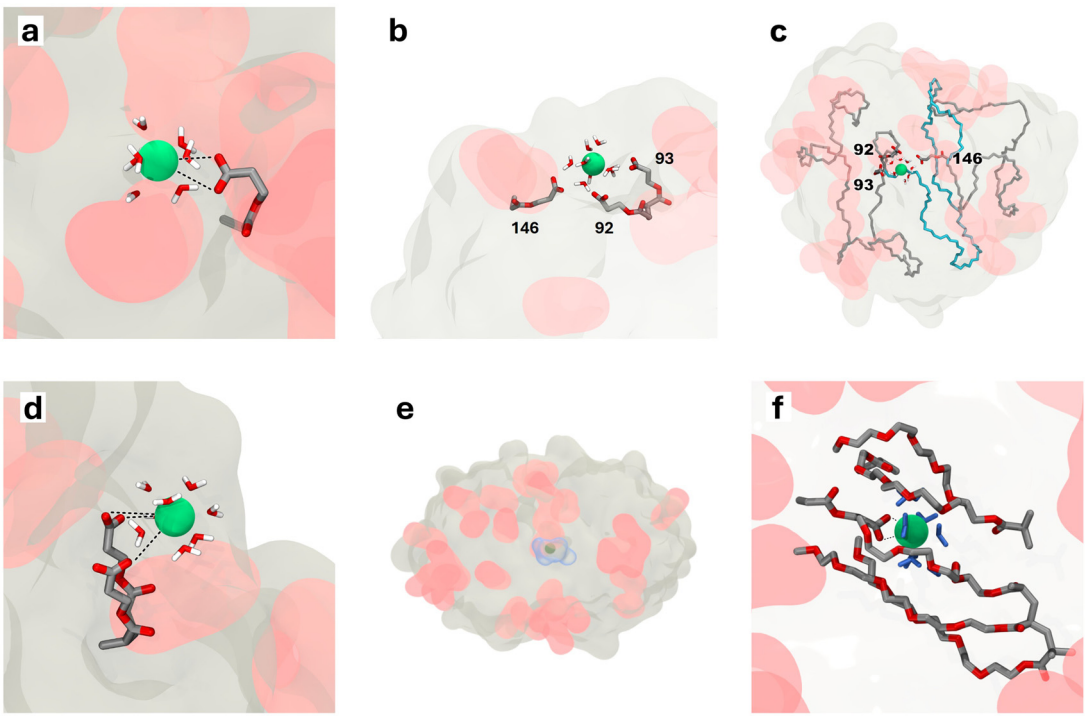

Fig. 3 Graphical illustration of the interactions of Ba(II) ions with poly(PEGMEMA-*co*-2-carboxyethyl acrylate) investigated by united atom molecular dynamics simulations (modified GROMOS 54a7 force field). (a) Illustration of one carboxylate group in the second barium coordination sphere. (b) Coordination of multiple carboxylates to the same barium ion, bridging distant regions of the macromolecular chain. (c) Zoomed-out contour between the distant carboxylates highlighted in cyan. Labels refer to the position along the chain. (d) Interactions of carboxylate monomers adjacent in the macromolecular chain with the same barium ion. (e) Encapsulation of a hydrated barium ion within the macromolecular chain. (f) Zoom-in to the encapsulated solvated barium ion. Color code: PEGMEMA grey contours, 2-carboxyethyl acrylate red contours, hydrogen white, carbon grey, oxygen red, barium green, water blue.

Detailed investigation of these rare events revealed encapsulation of a barium ion, together with its associated solvation shell, leading to the movement of the metal ion through the macromolecule before returning to the surrounding solvent (refer to Fig. 3e and f).

To probe the influence of metal coordination on the size of the macromolecules, radii of gyration were determined in the absence and presence of barium ions, respectively (refer to SI Table S7). In simulations with compact starting conformations, the macromolecules remained tightly compact throughout the entire simulation. In simulations with extended starting conformations, the macromolecules collapsed to form compact conformations within 100 ns and remained compact for the duration of the simulation (refer to SI Fig. S23). For SCNPs with extended starting conformations the radii of gyration continued to decrease slightly throughout the simulations, suggesting that further polymer compaction continues throughout the simulation time. Regardless of the initial conformation, the presence of Ba(II) ions did not influence the radius of gyration to a relevant extent. However, the presence of barium ions increased the rate of collapse of the macromolecules with extended initial conformations (refer to SI Fig. S24). It is hypothesized that the barium ions increase the interactions of functional groups from different regions of the SCNP, reducing the occurrence of flexible extended conformations through transient bridging interactions. This results in an apparent reduction in average size when an ensemble of macromolecules is considered, as is the case in size-sensitive experimental measurements such as SEC, DLS or DOSY.

In summary, the simulations demonstrate the critical effect of the carboxylate functionalities for the binding of the barium ions to the polymer and rationalize their effect on the polymer compaction. Further, the simulations indicate that the barium ions are reversibly bound to the macromolecules, making the SCNP compaction a dynamic equilibrium process.

Reversing SCNP folding by barium sulfate precipitation

The dynamic nature of the interactions of the barium ions with the macromolecules can be exploited to achieve targeted control over the folding state of the SCNPs. Specifically, control over the folding of **P1** and unfolding of **SCNP1-Ba** was reached by exploiting the well-known chemistry of barium in aqueous solution. As demonstrated in detail above, the coordination of polymer-bound carboxylate moieties to Ba(II) ions induced single-chain compaction. The latter was reversed by the addition of a sulfate source to an aqueous solution of **SCNP1-Ba**, leading to the precipitation of barium sulfate owing

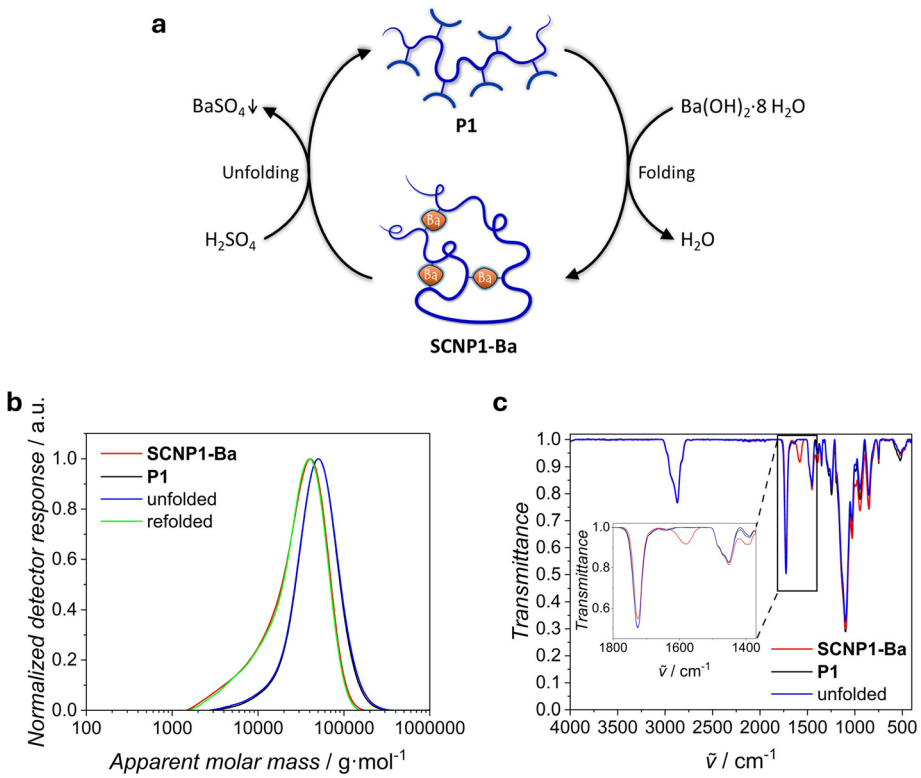

Fig. 4 Reversible control over the folding of polymer **P1** and unfolding of **SCNP1-Ba**. (a) Graphical illustration of the reversible folding of **P1** and unfolding of **SCNP1-Ba**. (b) Superimposed SEC chromatograms (THF, RI, PMMA cal.) of **P1** (black), **SCNP1-Ba** (red) and the products obtained after unfolding of **SCNP1-Ba** (blue) and refolding of the regenerated polymer (green). (c) FT-IR (ATR) spectra of **P1** (black), **SCNP1-Ba** (red) and the product obtained after unfolding of **SCNP1-Ba** (blue).

to its very small solubility product in water.[71] To regenerate the precursor polymer **P1**, it is additionally necessary to add a proton source to reprotonate the carboxylate moieties, making sulfuric acid the ideal candidate to achieve this in an elegant one-step procedure. The regenerated polymer can subsequently be employed in another folding reaction (refer to Fig. 4a).

The superimposed SEC chromatograms (refer to Fig. 4b), showing virtually no deviations between **P1** and the product regenerated after unfolding as well as **SCNP1-Ba** and the product obtained in a second folding step, respectively, demonstrate the excellent reversibility of the process on a macromolecular level. The reversibility on the functional group level is evident from the superimposed IR spectra of **P1**, **SCNP1-Ba** and the product obtained after unfolding of the latter (refer to Fig. 4c). Upon unfolding, the intensity of the carbonyl vibrational band at $\tilde{\nu}_{C=O}$ = 1724 cm^{-1} is recovered to the original value of **P1**, whereas it was reduced for **SCNP1-Ba**. Further, unfolding led to the disappearance of the bands associated with the asymmetric ($\tilde{\nu}_{as,COO}$ = 1583 cm^{-1}) and symmetric ($\tilde{\nu}_{s,COO}$ = 1410 cm^{-1}) carboxylate stretching vibrations.

Scanning transmission electron microscopy imaging of individual heavy metal atoms within SCNPs

Reproducible synthesis is a key factor determining the understanding and applications of single-chain technology. However, given the oftentimes synthetic unfeasibility of selective positioning of functionalities along a macromolecular chain, insights about the internal structure and distribution of functional moieties in SCNPs based on the repeat unit approach are highly desirable, yet challenging to obtain. For crystalline inorganic materials, atomic-level scanning transmission electron microscopy (STEM) imaging has become a routine investigation method due to the wider availability of aberration correction.[72] One of the major STEM imaging modes is annular dark field (ADF) or *Z*-contrast imaging, detecting electrons scattered to large angles due to Coulomb interactions with the sample atoms. In this imaging mode, the scattering signal intensity scales with the square of the atomic number of the sample element under investigation, enabling the detection of individual heavy atoms.[73] The contrast provided by the heavy barium atoms present in **SCNP1-Ba** makes the samples ideal for studying the internal structure of a metal-functionalized SCNP by STEM with single-atom sensitivity.

Initially, samples of **SCNP1-Ba** were prepared by dilution of the reaction mixture by a factor of one thousand and drop casting of the resulting solution on standard ultra-thin carbon film TEM grids followed by blotting of the excess solvent and drying. At low magnifications, barium-rich clusters were visible as bright areas (refer to Fig. 5a), and at higher magnifications individual barium atoms were identified as well-separated bright spots (refer to Fig. 5b).

From the STEM images, the number of barium ions per individual SCNP could in principle be obtained by direct counting of the visible atoms. The automated counting of individual well-separated atoms is a routine task,[74] however, the situation becomes drastically more complex when images are populated with overlapping atoms, rendering the identification of individual atoms challenging. To circumvent this challenge in the present case, the number of barium ions per nanoparticle was determined by integration of the signal intensity of identified individual barium clusters, which is justified by the direct proportionality of the measured dark field *Z*-contrast signal intensity to the number of atoms.[75] In detail, individual barium atoms were initially identified in high magnification images and their integrated signal intensity determined as the sum of the measured signal intensities within the considered area corrected by the average signal of the surrounding area to account for the background. Subsequently, the measured signal intensity within the area of a barium cluster identified in the high magnification image was integrated and the background corrected in the same way. The above approach enabled the quantification of the number of

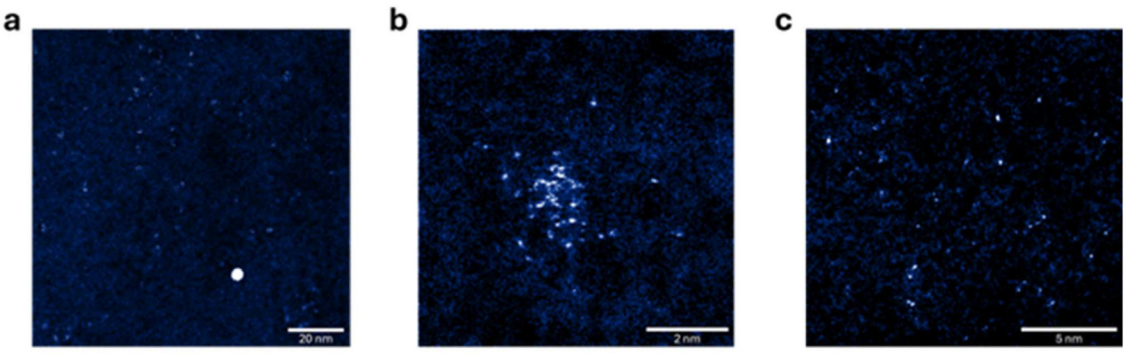

Fig. 5 ADF-STEM images of samples of **SCNP1-Ba** on carbon film. (a) Low magnification overview image showing bright individual clusters with high local barium concentrations. The sample was prepared by manual blotting and drying after deposition of an aqueous solution of **SCNP1-Ba** with a polymer concentration of 0.001 mg mL^{-1}. The large bright spot is a gold nanoparticle used as focus aid. (b) High magnification image of an individual cluster at the atomic level. (c) STEM image of a sample prepared employing a Gatan Cryoplunge 3 setup for blotting and drying after deposition of an aqueous solution of **SCNP1-Ba** with a polymer concentration of 0.01 mg mL^{-1}.

barium atoms within the identified cluster based on the previously determined intensity per barium atom. The obtained information was subsequently used to calculate the average integrated signal intensity per barium atom for the identified cluster at lower magnification. Based on these data, the number of barium atoms within other clusters visible in the low magnification image could be determined, enabling the analysis of a large number of clusters at low magnification. Evaluation of 472 clusters identified in low magnification images resulted in a mean and median barium content of 32 and 26 atoms, respectively (refer to SI Fig. S26).

It is noted that agglomeration of individual SCNPs upon drying throughout the sample preparation procedure could potentially lead to an overestimation of the number of barium ions per SCNP. To reduce this effect and establish a more reproducible sample preparation method, the application of a cryoplunge setup for blotting and subsequent drying was explored. The corresponding samples showed a drastically reduced density of bright areas on the substrate (refer to Fig. 5c). This is a result of the thinner and more homogeneous aqueous film upon blotting using the cryoplunge setup compared to manual blotting. The obtained STEM images show that every SCNP only contained one to two barium atoms, indicating that agglomeration upon drying might have indeed been a critical issue in the previously discussed images.

It is further noted that the sample preparation required a significant dilution of the reaction mixture to be capable of imaging individual clusters. Given the dynamic nature of the barium polymer interactions discussed in detail above, dilution is expected to shift the relevant equilibria, leading to a different number of barium ions per SCNP in the prepared microscopy samples compared to the situation at higher concentrations during synthesis.

Despite the criticality of sample preparation and imaging conditions for the precise quantification of the barium loading of individual SCNPs, atomic-level STEM imaging holds key potential for the exploration of the internal structure of metal-functionalized SCNPs not achievable by any other analytical technique. The advantage of this method is not only the high level of detail by resolving individual atoms, but also the possibility to produce statistically relevant data. Therefore, an in-depth understanding of metal polymer interactions can be achieved and structure–property relationships established in an unprecedented fashion, especially for catalytically active SCNPs with metal active sites, and metallopolymers in general.[76]

Conclusions

Barium-mediated single-chain nanoparticle (SCNP) compaction was achieved by the reaction of barium hydroxide octahydrate with the carboxylic acid functionalities of a copolymer of poly(ethylene glycol) methyl ether methacrylate and 2-carboxyethyl acrylate (Polymer **P1**).

The resulting nanoparticles **SCNP1-Ba** were characterized by infrared (IR) spectroscopy, and the successful intramolecular folding verified by size-exclusion chromatography (SEC), dynamic light scattering (DLS) and diffusion-ordered spectroscopy (DOSY). Sophisticated molecular dynamics simulations revealed the reversible nature of the barium polymer interactions in aqueous solutions of **SCNP1-Ba**, which opened a pathway towards targeted control over the polymer morphology by exploiting the low solubility of barium sulfate to reverse the SCNP folding reaction.

The high contrast provided by the heavy metal ions enabled the annular dark field (ADF) scanning transmission electron microscopy (STEM) imaging of individual barium atoms within **SCNP1-Ba**, providing in-depth insights into the number and distribution of metal ions on the level of individual SCNPs inaccessible by any other analytical technique.[77]

The findings reported herein pave the way for further explorations of the dynamic interactions between metals and polymers, aiding in the understanding of, for instance, structure–property relationships in the research area of metallopolymers or the role of metal cofactors in naturally occurring metalloproteins. The 2-carboxyethyl functionalities in our polymers are reminiscent of the side chain of glutamic acid, a vital component of a plethora of natural proteins, which can bind a variety of biologically relevant metal ions, such as Mg^{2+} or Ca^{2+}. Therefore, our SCNPs might find applications as model systems for the study of biologically meaningful dynamic metal–carboxylate interactions. The imaging of barium ions with single-atom sensitivity might give insights into metal–carboxylate interactions which cannot be assessed with the lighter alkaline earth ions.

Author contributions

S. G.: Conceptualization, methodology, formal analysis, investigation, writing – original draft, review & editing, visualization, project administration; J. A. K.: Conceptualization, methodology, formal analysis, investigation (TEM), writing – original draft, review & editing, visualization, project administration; A. Q.: Conceptualization, methodology, formal analysis, investigation (MD Simulations), writing – original draft, review & editing, visualization; J. O. H.: Writing – review & editing, supervision; K. M.: Resources; E. L.: Resources; D. G.: Resources; H. F.: Conceptualization, writing – review & editing, supervision, project administration; M. L. O.: Conceptualization, writing – review & editing, supervision; C. B.-K.: Conceptualization, writing – review & editing, supervision, project administration, funding acquisition; P. W. R.: Conceptualization, writing – review & editing, supervision, project administration, funding acquisition.

Conflicts of interest

There are no conflicts to declare.

Data availability

Experimental data and Python scripts used for the statistical analysis of the TEM data for this paper are available at

radar4chem [https://radar.products.fiz-karlsruhe.de/] at: https://doi.org/10.22000/10.22000/caett1857p1aq550. Python scripts, modified GROMOS 54a7 forcefield parameters and simulation input files for the MD simulations are available from GitHub: https://github.com/OMaraLab/BaSCNPs.

Supplementary information: methods, experimental procedures, supplemental analytical data, Fig. S1–S26, Tables S1–S13, Videos S1 and S2. See DOI: https://doi.org/10.1039/d5py00883b.

Acknowledgements

S. G. acknowledges funding by the Fonds der Chemischen Industrie in the form of a Kekulé fellowship (No. 110160). J. A. K. acknowledges the Deutsche Forschungsgemeinschaft (DFG, German Research Foundation) for his WBP fellowship (500289223) and WBP return grant (559314442). A. Q. and M. L. O. acknowledge support by resources and services provided by the National Computational Infrastructure (NCI) and the Pawsey Supercomputing Research Center, which is supported by the Australian Government, and the University of Queensland's Research Computing Centre (RCC). E. L. thanks the Leverhulme Trust for an Early Career Fellowship (ECF-2023-602). D. G. acknowledges the ARC Laureate Project FL160100089 for financial support and the ARC Project LE190100081 for establishing the aberration-corrected TEM facility at QUT. C. B.-K. and H. F. acknowledge the Australian Research Council (ARC) for a Laureate and DECRA fellowship, respectively. C. B.-K. and H. F. acknowledge continuous support by QUT's Centre for Materials Science. All authors acknowledge QUT's Central Analytical Research Facility (CARF) supported by QUT's Research Portfolio.

References

1 R. Feynman, There's Plenty of Room at the Bottom, *Eng. Sci.*, 1960, **23**, 22–36.
2 I. Khan, K. Saeed and I. Khan, Nanoparticles: Properties, applications and toxicities, *Arabian J. Chem.*, 2019, **12**, 908–931.
3 C. K. Lyon, A. Prasher, A. M. Hanlon, B. T. Tuten, C. A. Tooley, P. G. Frank and E. B. Berda, A brief user's guide to single-chain nanoparticles, *Polym. Chem.*, 2015, **6**, 181–197.
4 E. Harth, B. V. Horn, V. Y. Lee, D. S. Germack, C. P. Gonzales, R. D. Miller and C. J. Hawker, A Facile Approach to Architecturally Defined Nanoparticles via Intramolecular Chain Collapse, *J. Am. Chem. Soc.*, 2002, **124**, 8653–8660.
5 A. Tuteja, M. E. Mackay, C. J. Hawker, B. Van Horn and D. L. Ho, Molecular architecture and rheological characterization of novel intramolecularly crosslinked polystyrene nanoparticles, *J. Polym. Sci., Part B: Polym. Phys.*, 2006, **44**, 1930–1947.
6 J. N. Dobish, S. K. Hamilton and E. Harth, Synthesis of low-temperature benzocyclobutene cross-linker and utilization, *Polym. Chem.*, 2012, **3**, 857–860.
7 T. E. Dukette, M. E. Mackay, B. Van Horn, K. L. Wooley, E. Drockenmuller, M. Malkoch and C. J. Hawker, Conformation of Intramolecularly Cross-Linked Polymer Nanoparticles on Solid Substrates, *Nano Lett.*, 2005, **5**, 1704–1709.
8 O. Altintas, J. Willenbacher, K. N. R. Wuest, K. K. Oehlenschlaeger, P. Krolla-Sidenstein, H. Gliemann and C. Barner-Kowollik, A Mild and Efficient Approach to Functional Single-Chain Polymeric Nanoparticles via Photoinduced Diels–Alder Ligation, *Macromolecules*, 2013, **46**, 8092–8101.
9 I. Perez-Baena, I. Loinaz, D. Padro, I. García, H. J. Grande and I. Odriozola, Single-chain polyacrylic nanoparticles with multiple Gd(III) centres as potential MRI contrast agents, *J. Mater. Chem.*, 2010, **20**, 6916–6922.
10 A. R. de Luzuriaga, N. Ormategui, H. J. Grande, I. Odriozola, J. A. Pomposo and I. Loinaz, Intramolecular Click Cycloaddition: An Efficient Room-Temperature Route towards Bioconjugable Polymeric Nanoparticles, *Macromol. Rapid Commun.*, 2008, **29**, 1156–1160.
11 N. Ormategui, I. García, D. Padro, G. Cabañero, H. J. Grande and I. Loinaz, Synthesis of single chain thermoresponsive polymer nanoparticles, *Soft Matter*, 2012, **8**, 734–740.
12 A. R. de Luzuriaga, I. Perez-Baena, S. Montes, I. Loinaz, I. Odriozola, I. García and J. A. Pomposo, New Route to Polymeric Nanoparticles by Click Chemistry Using Bifunctional Cross-Linkers, *Macromol. Symp.*, 2010, **296**, 303–310.
13 H. Frisch, J. P. Menzel, F. R. Bloesser, D. E. Marschner, K. Mundsinger and C. Barner-Kowollik, Photochemistry in Confined Environments for Single-Chain Nanoparticle Design, *J. Am. Chem. Soc.*, 2018, **140**, 9551–9557.
14 A. E. Cherian, F. C. Sun, S. S. Sheiko and G. W. Coates, Formation of Nanoparticles by Intramolecular Cross-Linking:Following the Reaction Progress of Single Polymer Chains by Atomic Force Microscopy, *J. Am. Chem. Soc.*, 2007, **129**, 11350–11351.
15 A. Sanchez-Sanchez, D. A. Fulton and J. A. Pomposo, pH-responsive single-chain polymer nanoparticles utilising dynamic covalent enamine bonds, *Chem. Commun.*, 2014, **50**, 1871–1874.
16 L. Buruaga and J. A. Pomposo, Metal-Free Polymethyl Methacrylate (PMMA) Nanoparticles by Enamine "Click" Chemistry at Room Temperature, *Polymers*, 2011, **3**, 1673–1683.
17 J. B. Beck, K. L. Killops, T. Kang, K. Sivanandan, A. Bayles, M. E. Mackay, K. L. Wooley and C. J. Hawker, Facile Preparation of Nanoparticles by Intramolecular Cross-Linking of Isocyanate Functionalized Copolymers, *Macromolecules*, 2009, **42**, 5629–5635.

18 J. Wen, L. Yuan, Y. Yang, L. Liu and H. Zhao, Self-Assembly of Monotethered Single-Chain Nanoparticle Shape Amphiphiles, *ACS Macro Lett.*, 2013, **2**, 100–106.
19 O. Altintas, E. Lejeune, P. Gerstel and C. Barner-Kowollik, Bioinspired dual self-folding of single polymer chains via reversible hydrogen bonding, *Polym. Chem.*, 2012, **3**, 640–651.
20 O. Altintas, T. Rudolph and C. Barner-Kowollik, Single chain self-assembly of well-defined heterotelechelic polymers generated by ATRP and click chemistry revisited, *J. Polym. Sci., Part A: Polym. Chem.*, 2011, **49**, 2566–2576.
21 O. Altintas, P. Gerstel, N. Dingenouts and C. Barner-Kowollik, Single chain self-assembly: preparation of α,ω-donor–acceptor chains via living radical polymerization and orthogonal conjugation, *Chem. Commun.*, 2010, **46**, 6291–6293.
22 J. C. Nelson, J. G. Saven, J. S. Moore and P. G. Wolynes, Solvophobically driven folding of nonbiological oligomers, *Science*, 1997, **277**, 1793–1796.
23 D. D. Prabhu, K. Aratsu, Y. Kitamoto, H. Ouchi, T. Ohba, M. J. Hollamby, N. Shimizu, H. Takagi, R. Haruki, S. I. Adachi and S. Yagai, Self-folding of supramolecular polymers into bioinspired topology, *Sci. Adv.*, 2018, **4**, eaat8466.
24 P. F. Wu, A. Pietropaolo, M. Fortino, S. Shimoda, K. Maeda, T. Nishimura, M. Bando, N. Naga and T. Nakano, Non-uniform Self-folding of Helical Poly(fluorenevinylene) Derivatives in the Solid State Leading to Amplified Circular Dichroism and Circularly Polarized Light Emission, *Angew. Chem., Int. Ed.*, 2022, **61**, e202210556.
25 R. S. Lokey and B. L. Iverson, Synthetic Molecules That Fold into a Pleated Secondary Structure in Solution, *Nature*, 1995, **375**, 303–305.
26 O. Altintas and C. Barner-Kowollik, Single Chain Folding of Synthetic Polymers by Covalent and Non-Covalent Interactions: Current Status and Future Perspectives, *Macromol. Rapid Commun.*, 2012, **33**, 958–971.
27 I. Asenjo-Sanz, T. Claros, E. González, J. Pinacho-Olaciregui, E. Verde-Sesto and J. A. Pomposo, Significant effect of intra-chain distribution of catalytic sites on catalytic activity in "clickase" single-chain nanoparticles, *Mater. Lett.*, 2021, **304**, 130622.
28 J. L. Bohlen, B. Kulendran, H. Rothfuss, C. Barner-Kowollik and P. W. Roesky, Heterobimetallic Au(i)/Y(iii) single chain nanoparticles as recyclable homogenous catalysts, *Polym. Chem.*, 2021, **12**, 4016–4021.
29 S. Gillhuber, J. O. Holloway, H. Frisch, F. Feist, F. Weigend, C. Barner-Kowollik and P. W. Roesky, Ferrocene-driven single-chain polymer compaction, *Chem. Commun.*, 2023, **59**, 4672–4675.
30 S. Gillhuber, J. O. Holloway, K. Mundsinger, J. A. Kammerer, J. R. Harmer, H. Frisch, C. Barner-Kowollik and P. W. Roesky, Visible light photoflow synthesis of a Cu (ii) single-chain polymer nanoparticle catalyst, *Chem. Sci.*, 2024, **15**, 15280–15290.
31 A. E. Izuagbe, V. X. Truong, B. T. Tuten, P. W. Roesky and C. Barner-Kowollik, Visible Light Switchable Single-Chain Nanoparticles, *Macromolecules*, 2022, **55**, 9242–9248.
32 N. D. Knöfel, H. Rothfuss, C. Barner-Kowollik and P. W. Roesky, M24+ paddlewheel clusters as junction points in single-chain nanoparticles, *Polym. Chem.*, 2019, **10**, 86–93.
33 N. D. Knöfel, H. Rothfuss, P. Tzvetkova, B. Kulendran, C. Barner-Kowollik and P. W. Roesky, Heterobimetallic Eu (iii)/Pt(ii) single-chain nanoparticles: a path to enlighten catalytic reactions, *Chem. Sci.*, 2020, **11**, 10331–10336.
34 N. D. Knöfel, H. Rothfuss, J. Willenbacher, C. Barner-Kowollik and P. W. Roesky, Platinum(II)-Crosslinked Single-Chain Nanoparticles: An Approach towards Recyclable Homogeneous Catalysts, *Angew. Chem., Int. Ed.*, 2017, **56**, 4950–4954.
35 P. H. Maag, F. Feist, H. Frisch, P. W. Roesky and C. Barner-Kowollik, Fluorescent and Catalytically Active Single Chain Nanoparticles, *Macromolecules*, 2022, **55**, 9918–9924.
36 K. Mundsinger, A. Izuagbe, B. T. Tuten, P. W. Roesky and C. Barner-Kowollik, Single Chain Nanoparticles in Catalysis, *Angew. Chem., Int. Ed.*, 2024, **63**, e202311734.
37 J. Pinacho-Olaciregui, E. Verde-Sesto, D. Taton and J. A. Pomposo, Consecutive one-pot alkyne semihydrogenation/alkene dioxygenation reactions by Pt(ii)/Cu(ii) single-chain nanoparticles in green solvent, *Nanoscale*, 2024, **16**, 9742–9747.
38 H. Rothfuss, N. D. Knöfel, P. W. Roesky and C. Barner-Kowollik, Single-Chain Nanoparticles as Catalytic Nanoreactors, *J. Am. Chem. Soc.*, 2018, **140**, 5875–5881.
39 H. Rothfuss, N. D. Knöfel, P. Tzvetkova, N. C. Michenfelder, S. Baraban, A.-N. Unterreiner, P. W. Roesky and C. Barner-Kowollik, Phenanthroline—A Versatile Ligand for Advanced Functional Polymeric Materials, *Chem. – Eur. J.*, 2018, **24**, 17475–17486.
40 J. Rubio-Cervilla, E. González and J. A. Pomposo, Advances in Single-Chain Nanoparticles for Catalysis Applications, *Nanomaterials*, 2017, **7**, 341.
41 A. Sathyan, S. Croke, A. M. Pérez-López, B. F. M. de Waal, A. Unciti-Broceta and A. R. A. Palmans, Developing Pd(ii) based amphiphilic polymeric nanoparticles for pro-drug activation in complex media, *Mol. Syst. Des. Eng.*, 2022, **7**, 1736–1748.
42 J. Willenbacher, O. Altintas, P. W. Roesky and C. Barner-Kowollik, Single-Chain Self-Folding of Synthetic Polymers Induced by Metal–Ligand Complexation, *Macromol. Rapid Commun.*, 2014, **35**, 45–51.
43 J. Willenbacher, O. Altintas, V. Trouillet, N. Knöfel, M. J. Monteiro, P. W. Roesky and C. Barner-Kowollik, Pd-complex driven formation of single-chain nanoparticles, *Polym. Chem.*, 2015, **6**, 4358–4365.
44 T. M. Xiong, E. S. Garcia, J. Chen, L. Zhu, A. J. Alzona and S. C. Zimmerman, Enzyme-like catalysis by single chain nanoparticles that use transition metal cofactors, *Chem. Commun.*, 2022, **58**, 985–988.

45 A. Sathyan, T. Loman, L. Deng and A. R. A. Palmans, Amphiphilic polymeric nanoparticles enable homogenous rhodium-catalysed NH insertion reactions in living cells, *Nanoscale*, 2023, **15**, 12710–12717.
46 B. F. Patenaude, E. B. Berda and S. Pazicni, Probing secondary coordination sphere interactions within porphyrin-cored polymer nanoparticles, *Polym. Chem.*, 2022, **13**, 677–683.
47 A. E. Izuagbe, B. T. Tuten, P. W. Roesky and C. Barner-Kowollik, Light-driven folding of single polymer chains via metal-complexation, *Polym. Chem.*, 2024, **15**, 1955–1961.
48 S. Gillhuber, A. K. Finch, J. O. Holloway, H. Frisch, F. Weigend, C. Barner-Kowollik and P. W. Roesky, Introducing Photochemical Action Plots as a Tool for Unlocking On–Off Switchable Behavior in a Polymeric Eosin Y Photocatalyst, *Angew. Chem., Int. Ed.*, 2025, **64**, e202502890.
49 D. Arena, E. Verde-Sesto, I. Rivilla and J. A. Pomposo, Artificial Photosynthases: Single-Chain Nanoparticles with Manifold Visible-Light Photocatalytic Activity for Challenging "in Water" Organic Reactions, *J. Am. Chem. Soc.*, 2024, **146**, 14397–14403.
50 J. Pinacho-Olaciregui, E. Verde-Sesto, D. Taton and J. A. Pomposo, Gold Nanoclusters Synthesized within Single-Chain Nanoparticles as Catalytic Nanoreactors in Water, *Polymers*, 2024, **16**, 378.
51 J. Pinacho-Olaciregui, E. Verde-Sesto, D. Taton and J. A. Pomposo, Lanthanide-Based Single-Chain Nanoparticles as "Visual" Pass/Fail Sensors of Maximum Permissible Concentration of Cu(2+) Ions in Drinking Water, *Macromol. Rapid Commun.*, 2024, **45**, e2400116.
52 A. Sathyan, E. Archontakis, A. J. H. Spiering, L. Albertazzi and A. R. A. Palmans, Effect of Particle Heterogeneity in Catalytic Copper-Containing Single-Chain Polymeric Nanoparticles Revealed by Single-Particle Kinetics, *Molecules*, 2024, **29**, 1850.
53 A. Blazquez-Martín, E. Verde-Sesto, A. J. Moreno, A. Arbe, J. Colmenero and J. A. Pomposo, Advances in the Multi-Orthogonal Folding of Single Polymer Chains into Single-Chain Nanoparticles, *Polymers*, 2021, **13**, 293.
54 A. Levy, R. Feinstein and C. E. Diesendruck, Mechanical Unfolding and Thermal Refolding of Single-Chain Nanoparticles Using Ligand–Metal Bonds, *J. Am. Chem. Soc.*, 2019, **141**, 7256–7260.
55 N. Hosono, A. M. Kushner, J. Chung, A. R. A. Palmans, Z. Guan and E. W. Meijer, Forced Unfolding of Single-Chain Polymeric Nanoparticles, *J. Am. Chem. Soc.*, 2015, **137**, 6880–6888.
56 N. Wedler-Jasinski, T. Lueckerath, H. Mutlu, A. S. Goldmann, A. Walther, M. H. Stenzel and C. Barner-Kowollik, Dynamic covalent single chain nanoparticles based on hetero Diels–Alder chemistry, *Chem. Commun.*, 2017, **53**, 157–160.
57 F. Wang, H. Pu, M. Jin and D. Wan, Supramolecular Nanoparticles via Single-Chain Folding Driven by Ferrous Ions, *Macromol. Rapid Commun.*, 2016, **37**, 330–336.
58 F. Wang, H. Pu, Y. Ding, R. Lin, H. Pan, Z. Chang and M. Jin, Single-chain folding of amphiphilic copolymers in water via intramolecular hydrophobic interaction and unfolding triggered by cyclodextrin, *Polymer*, 2018, **141**, 86–92.
59 T. S. Fischer, D. Schulze-Sünninghausen, B. Luy, O. Altintas and C. Barner-Kowollik, Stepwise Unfolding of Single-Chain Nanoparticles by Chemically Triggered Gates, *Angew. Chem., Int. Ed.*, 2016, **55**, 11276–11280.
60 T. Mes, R. van der Weegen, A. R. A. Palmans and E. W. Meijer, Single-Chain Polymeric Nanoparticles by Stepwise Folding, *Angew. Chem., Int. Ed.*, 2011, **50**, 5085–5089.
61 F. Wang, H. Pu and X. Che, Voltage-responsive single-chain polymer nanoparticles via host–guest interaction, *Chem. Commun.*, 2016, **52**, 3516–3519.
62 T. S. Fischer, S. Spann, Q. An, B. Luy, M. Tsotsalas, J. P. Blinco, H. Mutlu and C. Barner-Kowollik, Self-reporting and refoldable profluorescent single-chain nanoparticles, *Chem. Sci.*, 2018, **9**, 4696–4702.
63 P. H. Maag, F. Feist, V. X. Truong, H. Frisch, P. W. Roesky and C. Barner-Kowollik, Visible-Light-Induced Control over Reversible Single-Chain Nanoparticle Folding, *Angew. Chem., Int. Ed.*, 2023, **62**, e202309259.
64 S. Babaoglu, D. Karaca Balta and G. Temel, Synthesis of photoactive single-chain folded polymeric nanoparticles via combination of radical polymerization techniques and Menschutkin click chemistry, *J. Polym. Sci., Part A: Polym. Chem.*, 2017, **55**, 1998–2003.
65 D. Kodura, H. A. Houck, F. R. Bloesser, A. S. Goldmann, F. E. Du Prez, H. Frisch and C. Barner-Kowollik, Light-fueled dynamic covalent crosslinking of single polymer chains in non-equilibrium states, *Chem. Sci.*, 2021, **12**, 1302–1310.
66 A. Alexander-Katz, H. Wada and R. R. Netz, Internal Friction and Nonequilibrium Unfolding of Polymeric Globules, *Phys. Rev. Lett.*, 2009, **103**, 028102.
67 Z. Han, S. L. Hilburg and A. Alexander-Katz, Forced Unfolding of Protein-Inspired Single-Chain Random Heteropolymers, *Macromolecules*, 2022, **55**, 1295–1309.
68 G. B. Deacon and R. J. Phillips, Relationships between the carbon-oxygen stretching frequencies of carboxylato complexes and the type of carboxylate coordination, *Coord. Chem. Rev.*, 1980, **33**, 227–250.
69 R. Munaweera, A. Quinn, L. Morrow, R. A. Morris and M. L. O'Mara, PolyConstruct: Adapting Biomolecular Simulation Pipelines for Polymers with PolyBuild, PolyConf, and PolyTop, *J. Chem. Inf. Model.*, 2025, **65**, 4918–4931.
70 H. J. C. Berendsen, J. R. Grigera and T. P. Straatsma, The missing term in effective pair potentials, *J. Phys. Chem.*, 1987, **91**, 6269–6271.
71 L. F. F. Corrêa, J. Hao, R. Neerup, S. Almeida, M. Shi, K. Thomsen and P. L. Fosbøl, Review of barium sulphate solubility measurements, *Geothermics*, 2022, **104**, 102465.
72 P. E. Batson, N. Dellby and O. L. Krivanek, Sub-ångstrom resolution using aberration corrected electron optics, *Nature*, 2002, **418**, 617–620.

73 M. P. Oxley, A. R. Lupini and S. J. Pennycook, Ultra-high resolution electron microscopy, *Rep. Prog. Phys.*, 2017, **80**, 026101.
74 L. Packman, B. Philippa, A. Pivrikas, P. L. Burn and I. R. Gentle, Reconstructing the 3D Coordinates of Guest: Host OLED Blends with Single Atom Resolution, *Small Methods*, 2024, **8**, 2301305.
75 A. A. Sousa and R. D. Leapman, Quantitative STEM mass measurement of biological macromolecules in a 300 kV TEM, *J. Microsc.*, 2007, **228**, 25–33.
76 A. Marathianos, A. Magiakos, Y. Han, A. Sanchez, R. Whitfield, J. Kammerer, A. Anastasaki, P. Wilson, J. P. Patterson, C. Barner-Kowollik and E. Liarou, Atomic-Scale Imaging of Polymers and Precision Molecular Weight Analysis, *J. Am. Chem. Soc.*, 2024, **146**, 34292–34297.
77 S. Gillhuber, *Synthesis and Characterization of Metal-Functionalized Single-Chain Polymer Nanoparticles as Versatile Catalytic Nanoreactors*, Dissertation, Karlsruhe Institute of Technology (KIT), Queensland University of Technology (QUT), 2024.